**JP1.11**

# CLOUD PHASE DETERMINATION IN THE ARCTIC USING AERI DATA

David D. Turner* and Steve A. Ackerman
CIMSS / University of Wisconsin – Madison, Madison, WI 53706

## 1. Introduction

Cloud-radiative processes in the Arctic have a large and significant effect on the global energy budget. Curry et al. [1996] have identified cloud phase as being one of the primary unknowns which effects the radiation budget in the Arctic. To correctly determine cloud properties such as particle size and condensed water path that dictate the cloud's radiative effects, the cloud phase must be accurately determined. However, the presence of highly reflecting snow and ice, together with a persistent temperature inversion that exists much of the year, hampers the ability to remotely detect cloud phase. This paper demonstrates that the use of far-infrared observations (between 17-20 μm) can help resolve ambiguities and improve IR cloud phase detection.

## 2. Approach

In the infrared, the refractive indices of liquid water and ice vary dramatically with wavelength, as shown in Figure 1. Many studies [e.g., Baum et al. 2000] have taken advantage of the differences in the imaginary refractive indices of water and ice between 8 and 12 μm to ascertain cloud phase. However, as shown in Fig 1, the indices of refraction are significantly different at 17-20 μm, with liquid water being more absorptive than ice. Using data from this wavelength region together with observations at 8 and 12 μm offers more information for accurate phase determination. The ground-based AERIs deployed during SHEBA and currently at the ARM NSA site have been extended such that high quality measurements can be made at these long wavelengths (i.e., at 18-24 μm).

We have investigated the ability to ascertain cloud phase by using downwelling brightness temperature observations at 9, 12, and 18 μm. Using gaseous optical depths calculated from the LBLRTM, a range of mixed phase clouds were simulated using DISORT. The total optical depth of the clouds ranged from 0.1 to 8, and the fraction of liquid water in the cloud ranged from 0 (all ice) to 1 (all liquid water) by increments of 0.1. This data was used to build an algorithm to identify the cloud phase. The simulation and the results of the cloud phase detection algorithm are shown in Fig 2. For this simulation, the cloud particles were uniformly mixed, although using adjacent layers (i.e., an ice cloud directly above a liquid water cloud or vice versa) does not significantly affect the results. The effective radius used for the liquid water droplets and ice crystals in this simulation is 7 μm and 21 μm, respectively, as suggested by in situ observations made by the cloud particle imager (CPI) flown on the NCAR C-130 during FIRE-ACE. Both phases used a gamma size distribution, again suggested by the CPI observations. The ice particles were modeled as hexagonal columns [Yang et al. 2001] for this simulation, but modeling the ice as spherical particles (using Mie code)

* Corresponding author address: David D. Turner, CIMSS / University of Wisconsin – Madison, Madison, WI 53706. Email: dturner@ssec.wisc.edu.

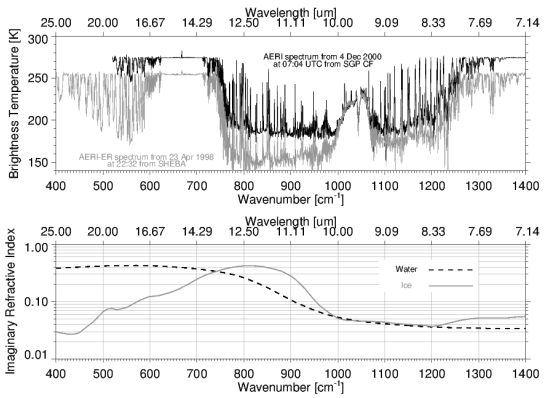


*Fig 1: Typical brightness temperature spectra observed by the AERIs at the ARM SGP site (black) and at SHEBA (gray). The lower curve shows the variation in the imaginary component of the refractive index of water and ice. Note the large change between the two at 12 μm versus 18 μm.*

does not significantly affect the results. The lower portion of Figure 2 indicates the makeup of the clouds in the simulation. The first sample was a clear sky case. The next 11 samples are for all ice clouds (open circles) where the optical depths range from 0.1 to 8.0. The next 11 samples are for liquid water clouds (closed circles) where the optical depths again range from 0.1 to 8.0. The remaining samples are all mixed phase. For each of the 11 intervals, the total optical depth of the cloud is fixed, with the fraction of the total optical depth attributed to ice ranging from 0.1 to 0.9. The upper panel of the figure shows various brightness temperature differences between the three channels used in the retrieval. The results of the phase determination algorithm are shown along the top of the top panel, where open circles indicate ice-only cloud, closed circles indicate a liquid-only cloud, open triangles indicate a mixed phase cloud, and an "x" symbol indicates the that cloud is too opaque for the algorithm to decide. The three-channel algorithm performs admirably for a majority of the mixed-phase cases, with errors in phase determination occurring when the cloud is mostly one phase. For example, when the liquid water optical depth is 90% of the total optical depth, the algorithm tends to call the cloud all liquid water versus mixed phase. The sensitivity of the phase determination algorithm to particle size of the liquid and ice particles has been investigated, with similar results for most reasonable effective radii. The technique is limited to optical depths less than approximately 5, but it is at these small optical depths that the combined radar/MWR techniques tend to lose their sensitivity due primarily to the sensitivity of the MWR. Therefore, this technique would be a valuable addition to the traditional radar/MWR techniques.

## 3. Initial results

The first step required before utilizing the infrared for cloud property studies, especially when the clouds are optically thin like many clouds in the Arctic, is to evaluate the ability

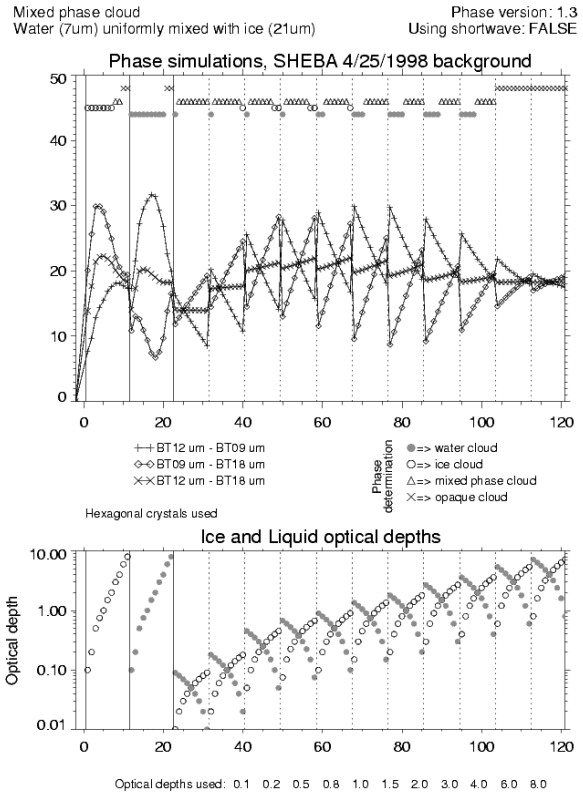


*Fig 2: Results from the mixed-phase cloud simulation to test the prototype cloud phase detection algorithm designed to use AERI observations. See text for details.*

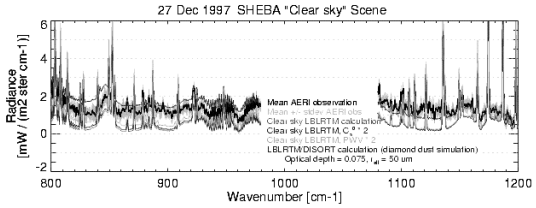


*Fig 3: "Clear –sky" comparison of observed (dark black line) minus calculated (gray line with smallest magnitude) downwelling radiance. Perturbing the water vapor continuum absorption or the amount of water vapor in the column (two gray lines immediately above the first calculation) does not explain the discrepancy between the observation and the calculation. However, inclusion of an optically thin ice cloud at the surface matches the observation much better.*

to model the clear sky. Comparisons between AERI observed and LBLRTM calculated radiance show a significant 1 mW / ($m^2$ ster $cm^{-1}$) residual in the 8-13 μm window that cannot be explained by uncertainties in the water vapor amount or the continuum absorption (Fig 3). This radiance residual translates into a 20-30 K error in brightness temperature. However, by inserting an ice cloud at the surface with an effective radius of 50 μm and a small optical depth explains the residuals fairly well. Using an iterative technique, the required cloud optical depth and effective radius was retrieved for each of the "confirmed" clear sky samples (using MMCR and DABUL data) during SHEBA. In all cases, the effective radius was 50 μm or greater, and the optical depth varied at values less than 0.1. These values agree with values of diamond dust reported by Witte [1968]. We are currently investigating the observations to rule out any calibration uncertainties before claiming these are diamond dust or ice fog observations.

The AERI phase determination algorithm was applied to several days of data collected during SHEBA. An example of the results is shown in Fig 4 for 21 April 1998. On this day, a small surface low was situated northeast of the ship, and winds were light and easterly at the surface, with stronger

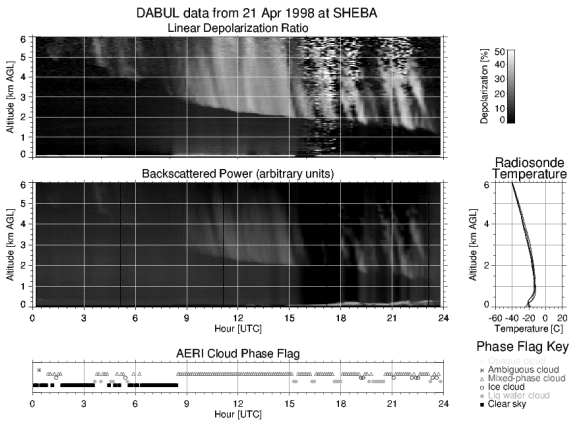


*Fig 4: Results of the AERI phase determination algorithm (bottom) with depolarization (top) and relative backscatter (middle) profiles observed by the DABUL on 21 April 1998. Radiosonde temperature profiles, collected every 6 h through the day, are also shown.*

winds from the southwest at upper levels. The DABUL lidar data, shown in Fig 4, indicate that a single layer cloud existed from 9-17 UTC with depolarization values ranging from 20-30%. These values are typically associated with scattering due to ice. The AERI phase detection algorithm indicated that this cloud was a mixed phase cloud, which is certainly possible due to the temperature of the cloud (~ -20K). From 17 – 24 UTC, a lower level cloud with low depolarization (which is usually associated with scattering from spherical liquid water drops) was overhead, along with the upper level cloud that had higher depolarization ratios that was becoming more porous. For times when the upper level cloud wasn't directly overhead, the AERI phase detection algorithm indicated the scene (which consisted only of the lower level cloud) was liquid water, while periods when both cloud levels where in the scene were identified as mixed phase.

## 4. Future work

As indicated above, this technique currently uses only data at three wavelengths, and therefore does not take advantage of the high spectral resolution of the AERI (other than avoiding spectral regions that have significant

absorption features of water vapor and other molecules). We are moving to extend this technique to include multiple wavelengths, including wavelengths in the 3-5 μm region where the refractive index of water and ice differ as compared to the 8-13 μm region to increase the sensitivity of the algorithm. We will also incorporate the cloud boundary information from the lidar and cloud radar to facilitate the retrieval of cloud liquid and ice water paths and effective radii. These data will then be used to build monthly and seasonal climatologies for the Arctic, using data from both the SHEBA and ARM NSA sites.

**Acknowledgements**

The U.S. Department of Energy's ARM program funded this research. We thank Ping Yang for the scattering properties of the hexagonal columns, and Bryan Baum for helpful discussions. We thank Janet Intrieri from NOAA/ETL for providing the DABUL data, as well as helping in its interpretation.

**References**

Baum, B.A., P.F. Soulen, K.I. Strabala, M.D. King, S.A. Ackerman, W.P. Menzel, and P. Yang, 2000: Remote sensing of cloud properties using MODIS airborne simulator imagery during SUCCESS: 2. Cloud thermodynamic phase. *J. Geophys. Res.*, **105**, 11781-11792.

Curry, J.A., W.B. Rossow, D. Randall, and J.L. Schramm, 1996: Overview of Arctic cloud and radiation characteristics. *J. Climate*, **9**, 1731-1764.

Whitte, H.J., 1968: Airborne observations of cloud particles and infrared flux density in the Arctic. MS Thesis, Dept. of Atmos. Sci., University of Washington, 102 pp.

Yang, P., B. Gao, B.A. Baum, Y.X. Hu, W.J. Wiscombe, S. Tsay, D.M. Winker, and S.L. Nasiri, 2001: Radiative properties of cirrus clouds in the infrared (8-13 μm) spectral region. J. *Quant. Spec. Rad. Trans.*, **70**, 473-504.